Available online at www.sciencedirect.com
ScienceDirect
Journal of Colloid and Interface Science 320 (2008) 582–589
JOURNAL OF Colloid and Interface Science
www.elsevier.com/locate/jcis

Electrokinetic flow of non-Newtonian fluids in microchannels

Claudio L.A. Berli [a,b,*], María L. Olivares [a,c]

[a] *INTEC (UNL-CONICET), Güemes 3450, 3000, Santa Fe, Argentina*
[b] *Departamento de Física, FBCB, UNL, Ciudad Universitaria, 3000, Santa Fe, Argentina*
[c] *Cátedra de Físicoquímica, FBCB, UNL, Ciudad Universitaria, 3000, Santa Fe, Argentina*

Received 12 November 2007; accepted 22 December 2007

Available online 6 February 2008

Abstract

A theoretical description of the electrokinetic flow of non-Newtonian fluids through slit and cylindrical microchannels is presented. Calculations are based on constitutive models of the fluid viscosity, and take into account wall depletion effects of colloids and polymer solutions. The resulting equations allow one to predict the flow rate and electric current as functions of the simultaneously applied electric potential and pressure gradients. It is found that (i) nonlinear effects induced by the shear-dependent viscosity are limited to the pressure-driven component of the flow, and (ii) the reciprocity between electroosmosis and streaming current is complied. Thus a generalized form of the force–flux relations is proposed, which is of interest in microfluidic applications.

Keywords: Electrokinetic flow; Non-Newtonian fluids; Nonlinear Onsager relations; Microfluidics

1. Introduction

In a variety of microfluidic applications, the transport of fluids is conducted by applying pressure differences (ΔP), electric potential differences (ΔV), or a combination of the two, which leads to coupled flows of matter and electricity, namely electrokinetic flow [1–3]. For simple fluids in micro- and nanoscale channels, the relationships between driving forces and conjugate fluxes are linear, and can be described by Onsager relations of nonequilibrium thermodynamics [4]. More precisely, the simultaneous flow rate Q and electric current I obey

$$\begin{bmatrix} Q \\ I \end{bmatrix} = \begin{bmatrix} L_{11} & L_{12} \\ L_{21} & L_{22} \end{bmatrix} \begin{bmatrix} \Delta P \\ \Delta V \end{bmatrix}, \tag{1}$$

where L_{11} is the hydrodynamic conductance, L_{12} represents electroosmosis, L_{21} comprises streaming phenomena, and L_{22} is the electric conductance. In particular, the matrix of coefficients is symmetric, $L_{12} = L_{21}$ (Onsager reciprocal relation [4–6]). Equation (1) is valid for isothermal systems, in steady state, and uniform concentration of species in the axial direction of channels. As these conditions are generally satisfied in practice, Eq. (1) allows one to describe microfluidic networks by analogy with electrical circuits [7–10]. Further, theoretical expressions of the coefficients can be written in terms of channel geometry, surface potential, and physicochemical properties of the fluid [8,11].

It is worth stressing that the linearity of the relations given above holds for simple fluids like aqueous electrolyte solutions, the viscosity of which is a constant coefficient (Newtonian behavior). However, complex fluids like polymer solutions, colloids, and cell suspensions are also manipulated in microfluidic applications, notably in the field of "laboratory-on-a-chip" [12,13]. The viscosity of these fluids depends on the shear rate developed in the microchannel (non-Newtonian behavior). Although Reynolds numbers are much lower than one in micro- and nanoscale channels, because of the small gap width, relatively high shear rates are attained in typical manipulations. Therefore, nonlinear effects are expected when complex fluids are subjected to electric potential and/or pressure gradients in microchannels (see, for instance, [14]). This is a crucial aspect for the design and operation of microfluidic chips. Nevertheless, one may observe that the subject has not been sufficiently treated in the literature: to the authors' knowledge, the only

* Corresponding author. Fax: +54 342 4550944.
E-mail address: cberli@ceride.gov.ar (C.L.A. Berli).

0021-9797/$ – see front matter
doi:10.1016/j.jcis.2007.12.032

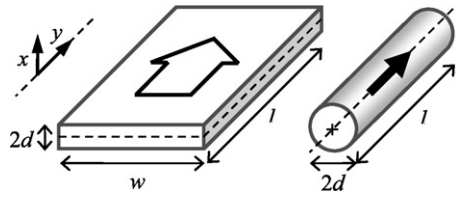

Fig. 1. Schematic representation of slit and cylindrical microchannels, including geometrical dimensions and the coordinate system used in calculations.

studies reported are those from Chakraborty et al. [15], who consider the electroosmotic flow of power-law fluids in slits, and Zimmerman et al. [16], who calculate numerically the electrokinetic flow of Carreau fluids in a T-shaped microchannel.

In this context, the aim of the present work is to investigate the form of the theoretical relations between fluxes and forces for the electrokinetic flow of complex fluids. For this purpose, theoretical aspects concerning the dynamics of non-Newtonian fluids and electrokinetic phenomena are outlined in Section 2. Then the mathematical model is formulated in Section 3. Finally, in Section 4, the resulting expressions of the flow rate and electric current are discussed, as well as the reciprocity between the coupling coefficients. Also in this section, a generalized form of the hydrodynamic conductance is proposed to extend the validity of Eq. (1).

2. Theory

2.1. Governing equations

In the framework of continuum fluid mechanics, the electrokinetic flow is described by a set of coupled equations that account for fluid velocity, pressure, ion concentration, and electric fields [17,18]. For the purposes of this analysis, axis and plane-symmetric flows are considered, which develop in cylindrical and slit microchannels, respectively (Fig. 1). Both fluid velocity and electric current are assumed to take place in the axial direction y, and vary in the transverse direction x. Such a unidirectional flow is attained in microchannels that present large aspect ratios, i.e., $l/d \gg 1$ (see geometrical definitions in Fig. 1). The present analysis also assumes that temperature is uniform throughout the flow domain. In practice, this is accomplished by using relatively low electric field strengths, which minimize the Joule effect in microchannels [1].

Electrokinetic effects are grounded on the existence of electrostatic charges in the solid–liquid interface [17,18]. The interfacial charge has associated an electric potential $\psi(x)$ that decreases and vanishes in the fluid due to the screening produced by counterions and other electrolyte ions in solution, which constitute the electrical double layer (EDL). The thickness of this layer is given by $\lambda = (\varepsilon k_B T/e^2 \sum_k z_k^2 n_{0,k})^{1/2}$, where $n_{0,k}$ is the bulk density of type k ions with valence z_k, e is the elementary charge, ε is the electric permittivity, k_B is the Boltzmann constant, and T is the absolute temperature [17,18]. There is also a potential $V(y)$ in the flow domain, which represents the potential externally applied to induce electroosmosis, or the one developed by streaming effects. Therefore the total electric potential involves two contributions, $\phi(x, y) = \psi(x) + V(y)$. This superposition is valid provided that (i) ion densities are uniform along the y-axis, as already required in the establishment of Eq. (1) (satisfying this condition is favored by the fact that microchannels are quite slim), and (ii) the EDL retains its equilibrium charge distribution even when the electrolyte solution flows. The last approximation is part of the standard electrokinetic model [18] and holds if $\Delta V/l$ is small in comparison with $\psi(d)/\lambda$, which is normally the case in practice (see also [6]).

The total electric potential in the flow domain is governed by Poisson equation, $\nabla^2\phi(x, y) = -\rho_e/\varepsilon$, where $\rho_e = e\sum_k z_k n_k$ is the electric charge density of the medium. The ion distributions n_k are obtained from transport equations that give the fluxes j_k of every species due to electrical forces, fluid convection and Brownian diffusion, i.e., Nerst–Planck equations [17]. For the flow geometries considered here (Fig. 1, $l/d \gg 1$),

$$j_{x,k} = -D_k\frac{\partial n_k}{\partial x} - z_k\nu_k n_k F\frac{\partial\psi}{\partial x}, \tag{2}$$

$$j_{y,k} = n_k u_y - z_k\nu_k n_k F\frac{\partial V}{\partial y}, \tag{3}$$

where D_k is the diffusion coefficient, ν_k is the ionic mobility, F is the Faraday constant, and u_y is the fluid velocity developed in the y-axis. Equation (2) neglects convective transport because there is no flow in the x-axis ($u_x = 0$), as stated in the formulation of the problem at the beginning of this section. Also for the problem posed here, Eq. (3) neglects diffusive transport since axial concentration gradients are assumed to be zero ($\partial n_k/\partial y \approx 0$), as discussed above. Furthermore, considering that channel walls are impermeable, there is no flux of ions in the x-axis ($j_{x,k} = 0$), thus Eq. (2) yields $n_k(x) = n_{0,k}\exp(-z_k e\psi/k_B T)$. Given these ion distributions, $\partial^2 V/\partial y^2 \approx 0$ and Poisson equation results,

$$\frac{1}{x^m}\frac{\partial}{\partial x}\left(x^m\frac{\partial\psi}{\partial x}\right) = -\frac{\rho_e(x)}{\varepsilon}. \tag{4}$$

Hereafter, m is used to describe either plane-symmetric ($m = 0$) or axisymmetric ($m = 1$) flow domains. For the geometries in Fig. 1, with $l/d \gg 1$, the steady-state flow of incompressible fluids is governed by the y-component of the momentum balance equation [17,18]:

$$\frac{\partial P}{\partial y} = \frac{1}{x^m}\frac{\partial(x^m\sigma_{xy})}{\partial x} - \rho_e\frac{\partial V}{\partial y}. \tag{5}$$

In this expression, σ_{xy} is the shear component of the stress tensor and $\partial P/\partial y = \partial(p - \rho g_y y)/\partial y$ is the total pressure gradient (p is the isotropic pressure, ρ is the fluid density, and g_y is the y-component of gravitational acceleration g). The last term on the right-hand side (RHS) of Eq. (5) represents the contribution of electric forces due to the presence of the electric field $-\partial V/\partial y$. One may observe that the flow in microchannels is entirely controlled by viscous forces [1–3]; hence the problem implies low Reynolds number hydrodynamics.

2.2. Fluid viscosity models

In order to asses the velocity profile $u_y(x)$, rheological information of the fluid must be included in Eq. (5), namely a

Table 1
Fluid viscosity models $\eta(\dot\gamma)$ and the corresponding fluidity functions $\Phi(\Delta P)$, where $B_m = (1+m)l/(d-\delta)$, with $m=0$ for slits and $m=1$ for cylinders

Model	$\eta(\dot\gamma)$	$\Phi(\Delta P)$
Newton	μ	$\frac{1}{\mu}$
Ostwald-de Waele (power law)	$\beta\dot\gamma^{\alpha-1}$	$\frac{3+m}{(1/\alpha+2+m)\beta}\left(\frac{\Delta P}{B_m\beta}\right)^{1/\alpha-1}$
Bingham	$\frac{\sigma_0}{\dot\gamma}+\eta_\infty$	$\frac{1}{\eta_\infty}\left[1-\frac{(3+m)}{(2+m)}\frac{B_m\sigma_0}{\Delta P}+\frac{1}{(2+m)}\left(\frac{B_m\sigma_0}{\Delta P}\right)^{3+m}\right]$
Eyring	$\eta_0\frac{\sinh^{-1}(\tau\dot\gamma)}{\tau\dot\gamma}$	$\frac{3+m}{\eta_0}\left(\frac{B_m\eta_0}{\Delta P\tau}\right)^{3+m}\left\{-m-\left(\frac{\Delta P\tau}{B_m\eta_0}\right)^m\sinh\left(\frac{\Delta P\tau}{B_m\eta_0}\right)+\left[m+\frac{1}{(1+m)}\left(\frac{\Delta P\tau}{B_m\eta_0}\right)^{1+m}\right]\cosh\left(\frac{\Delta P\tau}{B_m\eta_0}\right)\right\}$

constitutive relationship for the shear stress σ_{xy} in terms of the fluid velocity gradient $\dot\gamma_{xy}=\partial u_y/\partial x$. The following definition is used for the purposes [19],

$$\sigma_{xy}=\eta(\dot\gamma)\dot\gamma_{xy}, \tag{6}$$

where the fluid viscosity $\eta(\dot\gamma)$ is a function of the shear rate $\dot\gamma=|\dot\gamma_{xy}|$. In fact, the present modeling involves steady-state, isothermal, fully developed, rectilinear shear flows, which fulfil the requirements to attain viscometric flow conditions [19], where fluid viscosity depends on $\dot\gamma$ only. Typical examples of the function $\eta(\dot\gamma)$ are listed in Table 1. These viscosity models are named generalized Newtonian fluids [19], because of the analogy between the definition, $\sigma_{xy}=\eta(\dot\gamma)\dot\gamma_{xy}$, and the historical empiricism of Newton, $\sigma_{xy}=\mu\dot\gamma_{xy}$, where μ is a constant coefficient. In the power-law model of Ostwald-de Waele (Table 1), α is the flow behavior index and β is the consistency parameter. The plastic fluid of Bingham involves a yield stress σ_0, and a limiting viscosity η_∞ at high shear rates ($\dot\gamma\to\infty$). Finally, the Eyring model predicts Newtonian behavior at low shear rates ($\dot\gamma\to 0$), with viscosity η_0, and shear-thinning behavior when $\dot\gamma$ approaches the reciprocal of the relaxation time τ.

Generalized Newtonian fluids are illustrative of the most common behaviors found when complex fluids are subjected to steady shear flow and, at the same time, sufficiently simple to allow analytical solutions of the flow field in straight microchannels. It is worth adding, however, that these models cannot describe time-dependent responses (Eq. (6) implies that a given $\dot\gamma_{xy}$ results in a corresponding σ_{xy}, whose value does not change in time), nor viscoelastic phenomena. In this sense, one may note that elastic effects take relevance in systems that present contractions/expansions, curves, and mainly, unsteady flows (see [20] for an example in microfluidics involving pressure-driven flow). Modeling these situations is out of the scope of the present work, which is addressed to steady-state flow in straight microchannels.

2.3. Wall depletion effects related to non-Newtonian fluids

A crucial aspect to discuss here is that non-Newtonian behavior does not appear in simple liquids of low molecular weight, but in complex fluids like colloids, emulsions, macromolecular solutions, and gels [21]. The common feature in theses system is the presence of discrete entities at the micro/nanoscale. When a flow field is imposed, the equilibrium distribution of particles is disturbed by hydrodynamic forces, and immediately restored by Brownian motion. Non-Newtonian behavior is observed only if $\dot\gamma$ is high enough to overcome Brownian motion. Thus the critical shear rate $\dot\gamma_c$ required to attain non-Newtonian behavior can be estimated as the reciprocal of the time taken by particles to move diffusively a distance comparable to their size, $\tau\approx a^2/6D$, where a is particle radius and D is the Stokes–Einstein diffusion coefficient of particles. In water at room temperature, $a=10$ nm yields $\dot\gamma_c\sim 10^6\ \mathrm{s}^{-1}$, which is rather inaccessible in practice, while $a=100$ nm yields $\dot\gamma_c\sim 10^3\ \mathrm{s}^{-1}$, a shear rate value normally attained in microfluidic manipulations. Of course, increasing particle concentration, as well as the magnitude of particle–particle interactions, strongly influences the characteristic times [22], always leading to lower values of $\dot\gamma_c$.

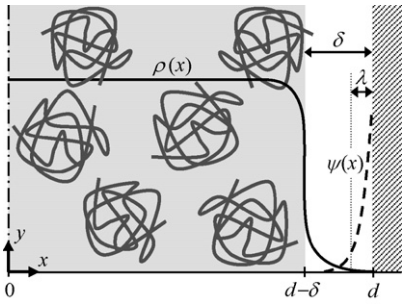

Fig. 2. Highly schematic representation of a macromolecular solution in a microchannel. The full curve represents the segment density profile of non-adsorbing polymers [24], and the dashed curve is the EDL potential (arbitrary drawings). Also in this scheme, λ is the EDL thickness and δ is the depletion layer thickness.

Therefore, non-Newtonian effects in microchannels imply the presence of discrete entities with sizes of several tenths of nanometers. The concern here is that these systems also exhibit wall depletion [23]: the concentration of nonadsorbing particles decreases steeply near smooth surfaces, leaving a depleted layer of pure solvent adjacent to the solid–liquid interface (Fig. 2). The depletion layer has a thickness δ of the order of the radius of gyration of macromolecules [24] or particles [25]. The viscosity of this layer is much lower than that of the bulk, which yields the apparent hydrodynamic slip, a phenomenon observed in polymer solutions [24,26], colloidal particles [25], emulsions [27], and notably in red blood cells suspensions [28,29] (these references are some of several examples found in the recent literature; see [23] for a comprehensive review of the subject).

The relevance of considering wall depletion is that electroosmotic and streaming effects take place in the region of the EDL, which extends a distance λ from the wall. For the ionic concentrations normally used in practice, $\lambda\approx$ 1–10 nm [17,18], while δ ranges from around 100 nm to 10 μm [23], depending on the fluid microstructure. Therefore, for a wide variety of non-Newtonian systems, the fact that $\lambda\ll\delta$ indicates that electrokinetic effects are confined to the region of pure solvent adjacent to the wall. Indeed, this is implicitly assumed in capillary electrophoresis of colloidal particles and cells [30,31],

where the electroosmotic flow is evaluated simply from the background electrolyte solution (the possible influence of suspension viscosity is disregarded).

In the present work, dispersed particles are assumed to be electrically neutral, in order to avoid both electrophoretic effects and the formation of an additional EDL at $x = d - \delta$. Besides, the size of discrete entities, say δ, needs to be much lower than d (one should note that Fig. 2 is highly schematic in this sense). Otherwise the continuum hypothesis breaks down, and statistical approaches must be used (see, for instance, [32]). Finally, it is worth noting that microchannel surfaces generally present certain degree of roughness, which may range from a few angstroms to some nanometers, depending on the material and fabrication process [1,3]. In the present modeling, solid–liquid interfaces are considered locally flat, as depicted in Fig. 2, or more precisely, with surface roughness much smaller than the EDL thickness λ.

3. Model formulation

On the basis of the arguments given above, the flow domain is divided in two zones as follows:

Zone I (gray in Fig. 2), which goes from the centerline up to the onset of the depletion layer. In this region the fluid is non-Newtonian and electrically neutral ($\rho_e \approx 0$), since the EDL potential is completely screened in the depletion layer. Thus Eq. (5) is rewritten as

$$\frac{\partial P}{\partial y} = \frac{\beta}{x^m}\frac{\partial}{\partial x}\left(x^m \left|\frac{\partial u_y}{\partial x}\right|^{\alpha-1}\frac{\partial u_y}{\partial x}\right), \quad 0 \leqslant x \leqslant (d-\delta), \tag{7}$$

where $\sigma_{xy} = \beta\dot{\gamma}^{\alpha-1}\dot{\gamma}_{xy}$ (power-law model; Table 1) was introduced to illustrate calculations. Nevertheless, the mathematical procedure is general and valid for any other model in the framework of Eq. (6). Of course, more sophisticated $\eta(\dot{\gamma})$ functions, like that of Carreau fluid [16,19], will demand numerical calculations to extract $u_y(x)$.

Zone II (white in Fig. 2), which comprises the depletion layer of pure solvent. Here the fluid is Newtonian, with viscosity μ_s, and ρ_e is associated to the EDL potential. Thus Eq. (5) with $\sigma_{xy} = \mu_s\dot{\gamma}_{xy}$ and ρ_e from Eq. (4) yields,

$$\frac{\partial P}{\partial y} = \frac{\mu_s}{x^m}\frac{\partial}{\partial x}\left(x^m\frac{\partial u_y}{\partial x}\right) + \frac{\varepsilon}{x^m}\frac{\partial}{\partial x}\left(x^m\frac{\partial \psi}{\partial x}\right)\frac{\partial V}{\partial y}, \quad (d-\delta) \leqslant x \leqslant d. \tag{8}$$

It is worth noting that d is the half-space between the plates in slits ($m = 0$), or the inner radius in cylindrical capillaries ($m = 1$), as shown in Fig. 1.

The boundary conditions required to solve the mathematical problem are written as follows:

$$x = 0, \qquad \sigma_{xy}^{(\mathrm{I})} = 0; \tag{9}$$

$$x = d - \delta, \qquad \sigma_{xy}^{(\mathrm{I})} = \sigma_{xy}^{(\mathrm{II})}, \qquad u_y^{(\mathrm{I})} = u_y^{(\mathrm{II})},$$

$$\partial\psi/\partial x = \psi = 0; \tag{10}$$

$$x = d, \qquad u_y^{(\mathrm{II})} = 0, \qquad \psi = \zeta. \tag{11}$$

The first condition (9) is a consequence of the symmetry of the flow geometries considered here. Matching conditions (10) for shear stress and fluid velocity are imposed at the surface connecting zones I and II. In addition, as discussed above, the EDL potential is assumed to vanish in zone I. The third condition (11) expresses that fluid velocity is zero at the channel wall, where $\psi(d)$ is identified as the electrokinetic ζ-potential [33].

Finally it should be noted that, although splitting the overall flow in two regions may oversimplify the physical problem, it is a reasonable approximation for the purposes of the present work. In fact, this mathematical procedure is widely used to describe complex flows in tubes, where a relevant example is the formulation made by Quemada [34] to derive the viscosity–volume fraction relationship of concentrated suspensions. Furthermore, if the fluid in zone I is also Newtonian, with viscosity $\mu \neq \mu_s$, the present modeling coincides with the "two fluid" approach used to describe the electroosmotic pumping of nonconducting fluids [35,36].

4. Results and discussions

4.1. Fluid velocity field

Solving Eqs. (7) and (8) with boundary conditions (9)–(11) yields,

$$u_y^{(\mathrm{I})} = \frac{[x^{1/\alpha+1} - (d-\delta)^{1/\alpha+1}]}{(1/\alpha+1)}\left(\frac{1}{(1+m)\beta}\frac{\partial P}{\partial y}\right)^{1/\alpha} + \frac{[(d-\delta)^2 - d^2]}{2(1+m)\mu_s}\frac{\partial P}{\partial y} + \frac{\varepsilon\zeta}{\mu_s}\frac{\partial V}{\partial y}, \tag{12}$$

$$u_y^{(\mathrm{II})} = \frac{(x^2-d^2)}{2(1+m)\mu_s}\frac{\partial P}{\partial y} + \frac{\varepsilon[\zeta - \psi(x)]}{\mu_s}\frac{\partial V}{\partial y}. \tag{13}$$

In these expressions, the terms involving $\partial P/\partial y$ account for the pressure-driven flow, and those with $\partial V/\partial y$ represent the electroosmotic flow. Further, the electric field is uniform in the axial direction and defined by the applied potential, $\partial V/\partial y = \Delta V/l$. The pressure gradient is also uniform along the channel; hence $\partial P/\partial y = \Delta P/l$.

The fluid velocity in zone I follows a nonlinear relation with the pressure gradient (power law in this case). In zone II instead, the classical linear relations of Newtonian fluids are recovered [1,11,17]. An illustration of the velocity profiles in slit microchannels is presented in Fig. 3. For these calculations, the EDL potential has been included according to Eq. (A.4), from Appendix A, and the ratio $\delta/d = 0.1$ was arbitrarily chosen. It is observed in Fig. 3 that, if $\Delta P = 0$ (pure electroosmotic flow), the fluid velocity is uniform throughout most of the cross-sectional area of the channel, and velocity gradients are limited to the region of the EDL adjacent to the interface. In other words, the interfacial layer of solvent drags the non-Newtonian fluid as a plug. When a pressure difference is applied, the rheological properties of each region become evident. Nevertheless, since the viscosity of the bulk fluid is larger than that of the solvent, most of the flow still occurs in the depletion layer.

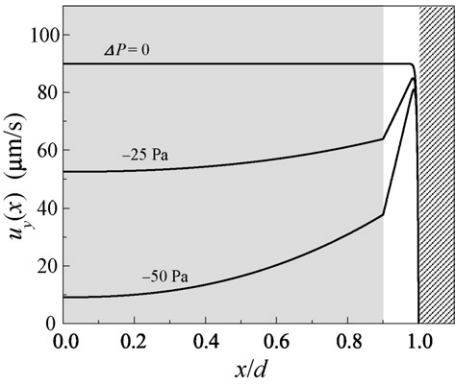

Fig. 3. Electrokinetic flow velocity of a power-law fluid ($\beta = 10$ mPa s$^\alpha$, $\alpha = 0.75$) in a slit microchannel, as a function of the relative distance x/d. The electric potential is fixed at $\Delta V = 50$ V, while the applied counterpressure varies as indicated in the figure. Numerical values used in calculations are: $l = 1$ cm, $d = 10$ μm, $\delta = 1$ μm, $\mu_s = 1$ mPa s, $\varepsilon = 7.1 \times 10^{-10}$ C^2/N m^2, $\zeta = -25$ mV, $\lambda = 30$ nm.

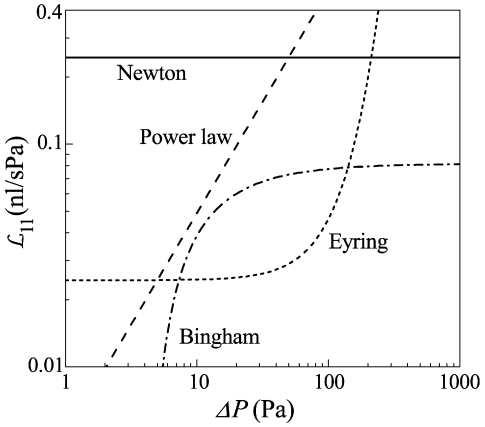

Fig. 4. Generalized hydrodynamic conductance $\mathcal{L}_{11}(\Delta P)$, as a function of pressure difference ΔP, in a cylindrical capillary of radius $d = 10$ μm and length $l = 1$ cm. Model parameters used in calculations are given in the text (Section 4.4). In all cases, $\delta \ll d$ was assumed.

4.2. Current density field

Once the velocity field is established, the electric current density is obtained as $J_y = e\sum_k z_k j_{y,k}$, where $j_{y,k}$ are given by Eq. (3). Therefore,

$$J_y^{(\mathrm{I})} = -s_0 \partial V/\partial y, \tag{14}$$

$$J_y^{(\mathrm{II})} = \rho_e u_y^{(\mathrm{II})} - s\,\partial V/\partial y, \tag{15}$$

where $s_0 = eF\sum_k z_k^2 \nu_k n_{0,k}$ is the electrical conductivity of the bulk, and $s = eF\sum_k z_k^2 \nu_k n_k(x)$ is the x-dependent conductivity due to EDL ion distributions in zone II (the ionic mobility ν_k is assumed to be the same in both regions). On the RHS of Eq. (14), the term accounting for the convective current ($\rho_e u_y^{(\mathrm{I})}$) is missing because $\rho_e \approx 0$ in zone I. Further, calculations here neglect the possible conductivity of the stagnant layer, i.e., Dukhin numbers much lower than one are assumed [33].

4.3. Force–flux relations

The flow rate Q and electric current I are obtained by integrating, respectively, the fluid velocity (Eqs. (12) and (13)) and the current density (Eqs. (14) and (15)) in the cross-sectional area of the channel. Equation (12) corresponds to power-law fluids; if one further considers other viscosity models in a common scheme, the resulting expressions are:

$$Q = -\frac{A_m(d-\delta)^2\Delta P}{(1+m)(3+m)l}\left\{\Phi(\Delta P) + \frac{1}{\mu_s}\left[\left(\frac{d}{d-\delta}\right)^{3+m} - 1\right]\right\} + \frac{A_m\varepsilon\zeta\Delta V[1+G_{1,m}(\psi,\delta)]}{l\mu_s}, \tag{16}$$

$$I = \frac{A_m\varepsilon\zeta\Delta P[1+G_{1,m}(\psi,\delta)]}{l\mu_s} - \frac{A_m\Delta V}{l} \times\left\{\left(\frac{\varepsilon\zeta}{d-\delta}\right)^2\frac{G_{2,m}(\psi,\delta)}{\mu_s} + s_0\big[1+G_{3,m}(\psi,\delta)\big]\right\}, \tag{17}$$

where A_m is the cross-sectional area of zone I, being $A_0 = 2w(d-\delta)$ for slits, and $A_1 = \pi(d-\delta)^2$ for cylindrical channels. In Eq. (16), $\Phi(\Delta P)$ is the fluidity function reported in Table 1 for different viscosity models. The geometrical functions $G_{1,m}(\psi,\delta)$, $G_{2,m}(\psi,\delta)$, and $G_{3,m}(\psi,\delta)$ depend on the EDL potential and depletion thickness, as reported in Appendix A.

It is observed that Q is nonlinear with ΔP due to the non-Newtonian character of the fluid, given by $\Phi(\Delta P)$ (Table 1). Nevertheless, as the nonlinearity is limited to the pressure-driven component of the flow, Eqs. (16) and (17) can be arranged in the matrix form of Eq. (1), by defining following coefficients:

$$\mathcal{L}_{11}(\Delta P) = -\frac{A_m(d-\delta)^2}{(1+m)(3+m)l} \times\left\{\Phi(\Delta P) + \frac{1}{\mu_s}\left[\left(\frac{d}{d-\delta}\right)^{3+m} - 1\right]\right\}, \tag{18}$$

$$L_{12} = L_{21} = \frac{A_m\varepsilon\zeta[1+G_{1,m}(\psi,\delta)]}{l\mu_s}, \tag{19}$$

$$L_{22} = -\frac{A_m}{l}\left\{\left(\frac{\varepsilon\zeta}{d-\delta}\right)^2\frac{G_{2,m}(\psi,\delta)}{\mu_s} - s_0\big[1+G_{3,m}(\psi,\delta)\big]\right\}. \tag{20}$$

In the framework of the generalized Newtonian fluid, $\mathcal{L}_{11}(\Delta P)$ may be regarded as a generalized hydrodynamic conductance that extends the validity of L_{11}, and hence of Eq. (1), to non-Newtonian fluids.

4.4. Generalized hydrodynamic conductance

Fig. 4 presents $\mathcal{L}_{11}$ vs ΔP in order to better visualize the influence of shear-dependent viscosities on the electrokinetic flow. A cylindrical microchannel is considered and $\delta \ll d$ is assumed for the sake of simplicity. Thus Eq. (18) reduces to $\mathcal{L}_{11}(\Delta P) = -\pi d^4\Phi(\Delta P)/8l$. The case where the bulk fluid is Newtonian ($\Phi = 1/\mu$) has been included as a reference, with $\mu = 1$ mPa s, which represents the viscosity of an aqueous electrolyte solution. Parameter values used in power-law, Eyring

and Bingham models were chosen for the purpose of illustration only, as described below.

Power-law fluids yield straight lines in log–log plots, the slopes of which depend on the flow index α. The example in Fig. 4 represents a shear-thinning fluid, with $\alpha = 0.5$ and $\beta = 10\ \text{mPa}\,\text{s}^{\alpha}$. These values are commonly found in dilute polymer solutions, such as carboxymethylcellulose or polyacrylamide. Eyring fluids typically represent colloidal suspensions. In this case, $\mathcal{L}_{11}$ exhibits a plateau at low ΔP, and then increases rapidly as ΔP increases. Parameter values used in Fig. 4 are $\eta_0 = 5$ mPa s and $\tau = 50$ ms, which can be obtained for example in semidilute suspensions of latex particles. For Bingham fluids, the overall response is also the increase of $\mathcal{L}_{11}$ with ΔP, but a critical value exists at low pressures (yield stress), at which the material virtually becomes a solid. In this case we used $\sigma_0 = 10$ mPa, which is of the order of the yield stress of blood, depending on cells concentration, and $\eta_\infty = 3$ mPa s.

Therefore, the generalized coefficient $\mathcal{L}_{11}(\Delta P)$ accounts for the rheological properties of the fluid through the associated fluidity function $\Phi(\Delta P)$. In a practical sense, the fact that $\mathcal{L}_{11}$ may change two orders of magnitude in the range 1–1000 Pa should not be ignored in microfluidic applications.

4.5. Onsager reciprocity

A relevant consequence of the formulation made in Section 3 is that electroosmosis depends on solvent viscosity only, and thus the expression of L_{12} (19) coincides with the well-established result of Newtonian fluids [11]. Accordingly, the streaming coefficient L_{21} is equal to L_{12}, which is a consistent result taken into consideration Onsager reciprocity of electrokinetic phenomena [4–6]. The electric conductance L_{22} (20) is also independent on the bulk rheology provided that the ionic mobilities are uniform in both flow regions. These results are characteristic of the analysis carried out in this work, which considers that electroosmotic and streaming phenomena take place in the depletion layer (the hypothesis has been also used in [16]). The relevance of this approach consists in the decoupling of electrokinetic and non-Newtonian effects. If one instead ignores the depletion layer, and considers that the fluid in the region of the EDL is non-Newtonian, then the predicted electroosmotic velocity is nonlinear with ΔV [15], the convective current is nonlinear with ΔP, and terms involving the crossed product $\Delta P \Delta V$ arise in both Q and I. In that case, additional research would be necessary to elucidate which symmetry relations are obeyed (see [5] for detailed discussions on nonlinear electrokinetic phenomena).

4.6. Cross-checking the results against a "single fluid" approach

As discussed in Section 2.3, wall depletion is inherent to fluids that exhibit non-Newtonian behavior. In our modeling, this phenomenon is taken into account by splitting the flow domain in two zones that differentiate each other from the fluid rheological properties. Instead, the interpretation of experimental data in the literature [23–27] is normally carried out by considering a "single fluid" that presents hydrodynamic slip at the wall. This alternative approach is studied in Appendix B, in order to cross-check our results. Equation (B.5) accounts for the electrokinetic velocity of power-law fluids with Navier slip condition and thin EDL.

It is worth noting here that Eqs. (12) and (13), as well as (14)–(20), are valid for arbitrary values of δ, while the approach in Appendix B involve $\delta \ll d$. Therefore, for the purposes of comparison, the prediction of our model needs to be written in the limit of small δ. That is, when $\delta \ll d$, zone I spans the entire flow domain and Eq. (12) results,

$$u_y = \frac{x^{1/\alpha+1} - d^{1/\alpha+1}}{(1/\alpha+1)} \left(\frac{1}{(1+m)\beta} \frac{\partial P}{\partial y} \right)^{1/\alpha} + \frac{\delta d}{(1+m)\mu_s} \frac{\partial P}{\partial y} + \frac{\varepsilon \zeta}{\mu_s} \frac{\partial V}{\partial y}. \tag{21}$$

Of course, zone II vanishes in this asymptotic situation and Eq. (13) does not contribute to the fluid velocity.

A simple inspection indicates that Eqs. (21) and (B.5) differ in the second term on the RHS only. Further calculations show that Eqs. (21) and (B.5) are indeed equivalent, provided that Navier slip length is expressed $b = \delta\eta/\mu_s$ (in following these straightforward calculations note that $d(\partial P/\partial y)/(1+m) = \sigma_{xy}$ is the shear stress at the interface). Moreover, it is relevant to point out that $b = \delta\eta/\mu_s$ is the slip length reported for macromolecular solutions with bulk viscosity η [24,26]. This remarkable result indicates the consistency of the modeling carried out here to describe the electrokinetic flow of non-Newtonian fluids.

5. Summary

A theoretical description of the electrokinetic flow of complex fluids in microchannels is presented. The resulting equations allow one to predict the flows of matter and electricity as functions of the simultaneously applied electric potential and pressure gradients, for different non-Newtonian fluids, through both slit and cylindrical microchannels. Calculations take into account the depletion of the disperse phase at channel walls, and consistently assume that electrokinetic phenomena occur in the interfacial layer of pure solvent. The advantage of this consideration is the decoupling of electrokinetic and non-Newtonian effects, which yields two relevant results. First, nonlinear effects induced by the shear-dependent viscosity are confined to the function $\mathcal{L}_{11}(\Delta P)$, which is defined to be a generalized hydrodynamic conductance. Thus the matrix form of the force–flux relations (characteristic of linear systems) is extended to non-Newtonian fluids. Second, neither the electroosmotic component of the flow nor the streaming component of the current are affected by the bulk rheology. As a consequence, the matrix of coefficients is symmetric ($L_{12} = L_{21}$) and Onsager fundamental theorem is complied. One may finally conclude that the analysis carried out in this work helps to better rationalize the dynamics of complex fluids in microchannels, which is of interest in microfluidics, as well as in related fields like capillary electrophoresis and flow through porous media.

Acknowledgments

The authors thank Agencia Nacional de Promoción Científica y Tecnológica (ANPCyT) and Consejo Nacional de Investigaciones Científicas y Técnicas (CONICET), Argentina, for the financial aid received.

Appendix A. Geometrical functions

The dimensionless geometrical functions appearing in Eqs. (16)–(20) are:

$$G_{1,m}(\psi,\delta)=\frac{1+m}{(d-\delta)^{1+m}}\int_{d-\delta}^{d}\left(1-\frac{\psi(x)}{\zeta}\right)x^m\,dx, \tag{A.1}$$

$$G_{2,m}(\psi,\delta)=\frac{1+m}{(d-\delta)^{m-1}}\int_{d-\delta}^{d}\left[\frac{\partial}{\partial x}\left(\frac{\psi(x)}{\zeta}\right)\right]^2 x^m\,dx, \tag{A.2}$$

$$G_{3,m}(\psi,\delta)=\frac{1+m}{(d-\delta)^{1+m}}\times\int_{d-\delta}^{d}\frac{\sum_k z_k^2\nu_k n_{0,k}\exp[-z_k e\psi(x)/k_{\mathrm{B}}T]}{\sum_k z_k^2\nu_k n_{0,k}}x^m\,dx, \tag{A.3}$$

where d is the half-space between the plates in slits ($m=0$) or the inner radius in cylindrical capillaries ($m=1$). It is easily seen that all of these functions vanish when $\delta\ll d$. For the general case, calculations require the EDL potential $\psi(x)$ from Eq. (4), which normally implies numerical procedures. In particular, systems involving relatively low surface potentials ($|\zeta|\leqslant 50$ mV) allow one to derive analytic $\psi(x)$ functions, which simplify the integrations of Eqs. (A.1)–(A.3). In fact, considering symmetric electrolytes ($z_+=-z_-\equiv z$) and using the Debye–Hückel approximation, the solution of Eq. (4) for a flat interface is [17,18]

$$\psi(x)=\zeta\exp\bigl[-(d-x)/\lambda\bigr]. \tag{A.4}$$

This result allows one to obtain analytic expressions of the geometrical functions for slit microchannels,

$$G_{1,0}=\frac{\delta+\lambda(e^{-\delta/\lambda}-1)}{(d-\delta)}, \tag{A.5}$$

$$G_{2,0}=\frac{d-\delta}{2\lambda}\bigl(1-e^{-2\delta/\lambda}\bigr), \tag{A.6}$$

$$G_{3,0}=\frac{\delta+\lambda\gamma Z(1-e^{-\delta/\lambda})}{(d-\delta)}. \tag{A.7}$$

In Eq. (A.7), $\gamma=(\nu_+-\nu_-)/(\nu_++\nu_-)$ and $Z=e\zeta/k_{\mathrm{B}}T$. It is observed that the EDL thickness λ is the controlling parameter. For the asymptotic case where $\lambda\ll\delta$, $G_{1,0}\to\delta/(d-\delta)$, $G_{2,0}\to(d-\delta)/2\lambda$, and $G_{3,0}\to\delta/(d-\delta)$. Finally, although Eqs. (A.5)–(A.7) are strictly valid for slits, they may be good approximations for cylindrical capillaries as well, taking into account that $\lambda<\delta<d$ implies a roughly flat EDL.

Appendix B. "Single fluid" approach with hydrodynamic slip at the wall

Here we study the limiting case where the depletion layer δ is negligibly small in comparison with channel depth d, but still larger that the EDL thickness λ. Under the circumstances, one may consider that the non-Newtonian fluid occupies the entire flow domain ($0<x<d$; Fig. 1), hence a "single fluid" approach is used to calculate the velocity profile. In addition, the layer of solvent adjacent to the wall is taken into account by including an apparent hydrodynamic slip, as it is usually indicated in the literature [23–27]. Since $\lambda<\delta$, the fluid is also electrically neutral, except in the close vicinity of the charged interface. Thus the thin EDL approximation applies [1,10], which allows one to evaluate pressure and electrically driven flows separately: (i) The pressure-driven component of the fluid velocity, $u_y^{(\mathrm{p})}$, is obtained from Eq. (5) with $\rho_{\mathrm{e}}\approx 0$ and $\sigma_{xy}=\beta\dot\gamma^{\alpha-1}\dot\gamma_{xy}$ (power-law fluids), that is

$$\frac{\partial P}{\partial y}=\frac{\beta}{x^m}\frac{\partial}{\partial x}\left(x^m\left|\frac{\partial u_y^{(\mathrm{p})}}{\partial x}\right|^{\alpha-1}\frac{\partial u_y^{(\mathrm{p})}}{\partial x}\right). \tag{B.1}$$

For the problem posed, boundary values are written as follows:

$$x=0,\qquad \partial u_y^{(\mathrm{p})}/\partial x=0, \tag{B.2}$$

$$x=d,\qquad u_y^{(\mathrm{p})}=b\bigl(\partial u_y^{(\mathrm{p})}/\partial x\bigr). \tag{B.3}$$

In particular, Eq. (B.3) represents Navier conditions for hydrodynamic slip at the wall, where b is the Navier slip length [3,24]. (ii) The electrically driven component of the fluid velocity is directly

$$u_y^{(\mathrm{e})}=\frac{\varepsilon\zeta}{\mu_{\mathrm{s}}}\frac{\partial V}{\partial y}, \tag{B.4}$$

which describes the electroosmotic flow for $\lambda\ll d$ [1,17,18,33]. It should be observed that Eq. (B.4) includes the solvent viscosity μ_{s} because electroosmosis is confined to the depletion layer.

Therefore, solving Eqs. (B.1)–(B.3) for $u_y^{(\mathrm{p})}$ and then adding $u_y^{(\mathrm{e})}$ yields,

$$u_y=\frac{x^{1/\alpha+1}-d^{1/\alpha+1}}{(1/\alpha+1)}\left(\frac{1}{(1+m)\beta}\frac{\partial P}{\partial y}\right)^{1/\alpha}+b\left(\frac{d}{(1+m)\beta}\frac{\partial P}{\partial y}\right)^{1/\alpha}+\frac{\varepsilon\zeta}{\mu_{\mathrm{s}}}\frac{\partial V}{\partial y}. \tag{B.5}$$

This expression represents the electrokinetic velocity profile of power-law fluids that slip at the wall, under the thin EDL approximation. Similar calculations can be carried out for other viscosity models in the framework of Eq. (6).

References

[1] D. Li, Electrokinetics in Microfluidics, Elsevier, London, 2004.
[2] H.A. Stone, A.D. Stroock, A. Adjari, Annu. Rev. Fluid Mech. 36 (2004) 381.
[3] P. Tabeling, Introduction to Microfluidics, Oxford Univ. Press, New York, 2005.

[4] S.R. De Groot, Thermodynamics of Irreversible Processes, North-Holland, Amsterdam, 1951.
[5] R.P. Rastogi, R.C. Srivastava, S.N. Singh, Chem. Rev. 93 (1993) 1945.
[6] E. Brunet, A. Adjari, Phys. Rev. E 69 (2004) 016306.
[7] A. Adjari, C. R. Phys. 5 (2004) 539.
[8] X. Xuan, D. Li, J. Micromech. Microeng. 14 (2004) 290.
[9] A.N. Chatterjee, N.R. Aluru, J. Microelectromech. Syst. 14 (2005) 81.
[10] C.L.A. Berli, Microfluid Nanofluid, in press, doi:10.1007/s10404-007-0191-2.
[11] C.L.A. Berli, Colloids Surf. A 301 (2007) 271.
[12] G.M. Whitesides, Nature 442 (2006) 367.
[13] C.D. Chin, V. Linder, S.K. Sia, Lab Chip 7 (2007) 41.
[14] A. Groisman, M. Enzelberger, S.R. Quake, Science 300 (2003) 955.
[15] S. Das, S. Chakraborty, Anal. Chim. Acta 559 (2006) 15.
[16] W.B. Zimmerman, J.M. Rees, T.J. Craven, Microfluid Nanofluid 2 (2006) 481.
[17] R.F. Probstein, Physicochemical Hydrodynamics, Butterworths, New York, 1989.
[18] R.J. Hunter, Foundations of Colloid Science, vols. I and II, Clarendon, Oxford, 1992.
[19] R.B. Bird, R. Armstrog, O. Hassager, Dynamics of Polymeric Liquids, vol. I, Wiley, New York, 1977.
[20] J.A. Pathak, D. Ross, K.B. Migler, Phys. Fluids 16 (2004) 4028.
[21] R.G. Larson, The Structure and Rheology of Complex Fluids, Oxford Univ. Press, New York, 1999.
[22] D. Quemada, C.L.A. Berli, Adv. Colloid Interface Sci. 98 (2002) 51.
[23] H.A. Barnes, J. Non-Newton. Fluid Mech. 56 (1995) 221.
[24] R. Tuinier, T. Taniguchi, J. Phys. Condens. Matter 17 (2005) L9.
[25] P.J.A. Hartman Kok, S.G. Kazarian, B.J. Briscoe, C.J. Lawrence, J. Colloid Interface Sci. 280 (2004) 511.
[26] G. Degré, P. Joseph, P. Tabeling, S. Lerouge, M. Cloitre, A. Adjari, Appl. Phys. Lett. 89 (2006) 024104.
[27] L. Bécu, P. Grondin, A. Colin, S. Manneville, Colloids Surf. A 263 (2004) 146.
[28] S. Chakraborty, Lab Chip 5 (2005) 421.
[29] R.D. Jäggi, R. Sandoz, C.S. Effenhauser, Microfluid Nanofluid 3 (2007) 47.
[30] W.-H. Lu, W.-H. Deng, S.-T. Liu, T.-B. Chen, P.-F. Rao, Anal. Biochem. 314 (2003) 194.
[31] M.A. Rodríguez, D.W. Armstrong, J. Chromatogr. B 800 (2004) 7.
[32] X. Fan, N. Phan-Thien, N.T. Yong, X. Wu, D. Xu, Phys. Fluids 15 (2003) 11.
[33] A.V. Delgado, F. González-Caballero, R.J. Hunter, L.K. Koopal, J. Lyklema, J. Colloid Interface Sci. 309 (2007) 194.
[34] D. Quemada, Rheol. Acta 16 (1977) 82.
[35] Y. Gao, T.N. Wong, C. Yang, K.T. Ooi, J. Colloid Interface Sci. 284 (2006) 306.
[36] J.S.H. Lee, I. Barbulovic-Nad, Z. Wu, X. Xuan, D. Li, J. Appl. Phys. 99 (2006) 054905.